



**University
of Dayton**

AEE 546 — Finite Element Analysis I

Department of Mechanical and Aerospace Engineering

Finite Element Analysis of a Torque Arm

Author:

Evan Burke

Instructor:

Dr. Thomas Whitney

7 December 2022

Contents

1	Introduction	3
2	Mesh Convergence	5
3	Results	6
4	Redesign	12
5	Summary and Conclusions	14
Appendix A	References	16
Appendix B	Safety Factor Calculation	17

List of Figures

1	Dimensioned torque arm sketch	3
2	Preload BC and loads shown on top, oscillating BC and loads shown on bottom.	4
3	Coarse, converged, and finest mesh.	6
4	Contour plots of Von Mises stress for initial and converged meshes	6
5	Contours of Von Mises stress for baseline preload	7
6	Contours of Von Mises stress for baseline oscillating load	8
7	Net reaction force during preload shows agreement with applied load	8
8	Net reaction force during oscillating load shows agreement with applied load	9
9	Contour plot of combined Von Mises stresses	9
10	Contour plot of combined Von Mises stresses with failed regions highlighted	10
11	Contour plot of Gerber equation values	11
12	Contour plot of Gerber equation values with failed regions highlighted	11
13	Contours of Von Mises stress for redesigned preload	12
14	Contours of Von Mises stress for redesigned oscillating load	13
15	Contour plot of combined Von Mises stresses on redesigned model	13
16	Contour plot of Gerber equation values on redesigned model	14

List of Tables

1	Preload mesh convergence history	5
2	Oscillating mesh convergence history	5

1 Introduction

A torque arm is a mechanical element that converts axial motion into rotational motion. This analysis examines the yield and endurance strength of a simplified torque arm subject to a constant axial preload and an oscillating vertical load. All modeling is performed using the finite element code *Abaqus*, assuming a 2-D plane stress model and varying model thicknesses on various portions of the torque arm. The key metric of interest for the analysis is the maximum stress experienced by the torque arm, rather than strains or displacements under load.

The geometry of the analytical model is shown in figure 1, with all units in mm. The circular regions surrounding the holes in the torque arm are known as *bushings* and are modeled with a larger thickness than the rest of the body. In an actual torque arm there would be a smooth transition between the two regions, but for the purposes of this simplified analysis we represent them with a discontinuous transition in thickness. This modeling decision implicitly assumes that the critical stresses of interest do not lie in the region of the bushings.

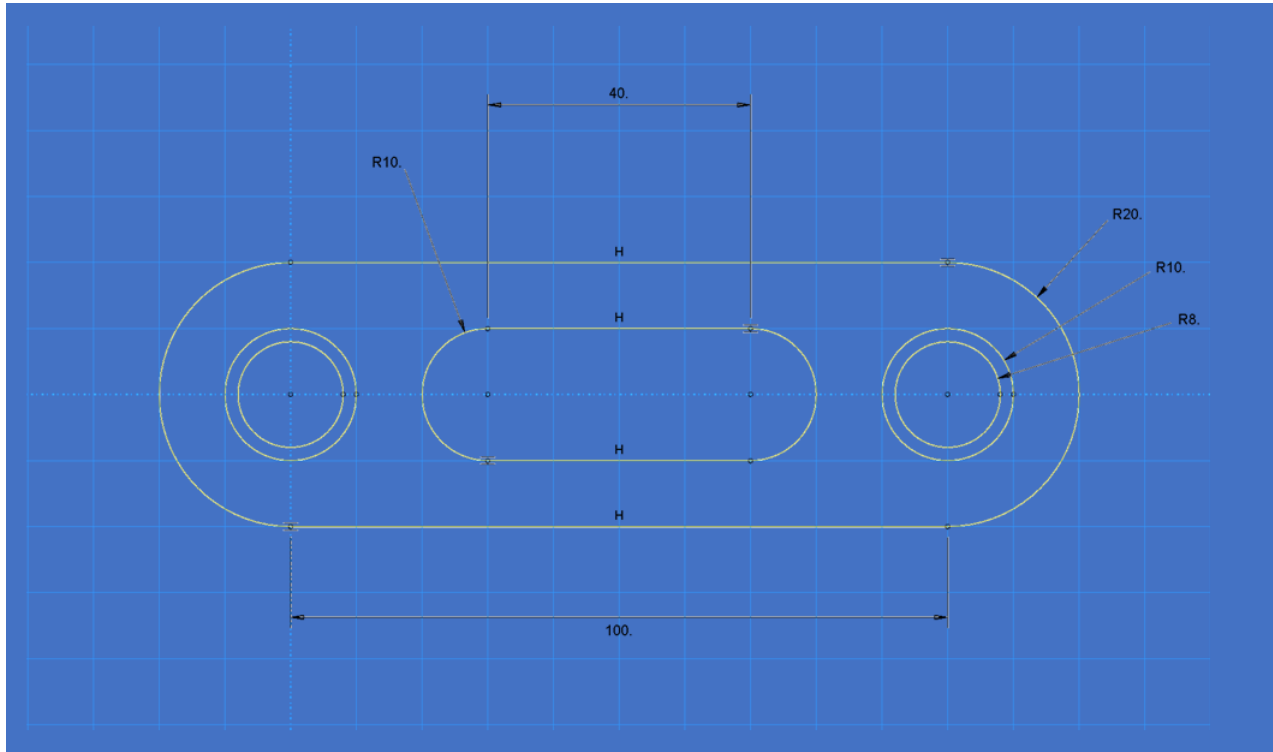


Figure 1: Dimensioned torque arm sketch

The sole boundary condition applied to the model is on the left hole — an *encastre* boundary condition constraining all nodal translations and rotations. Loads are applied as pressures

distributed over full surface area of the right hole — this method of applying the force is not fully physically accurate but does not undermine the analysis of the critical stresses present in the torque arm. The axial preload is a force with magnitude 4500 N while the oscillating component is ± 900 N. The resulting tractions applied to the right hole are 11.19 MPa and 2.24 MPa respectively. BCs and loads are shown in figure 2 — note that the preload and oscillating load are applied in distinct steps.

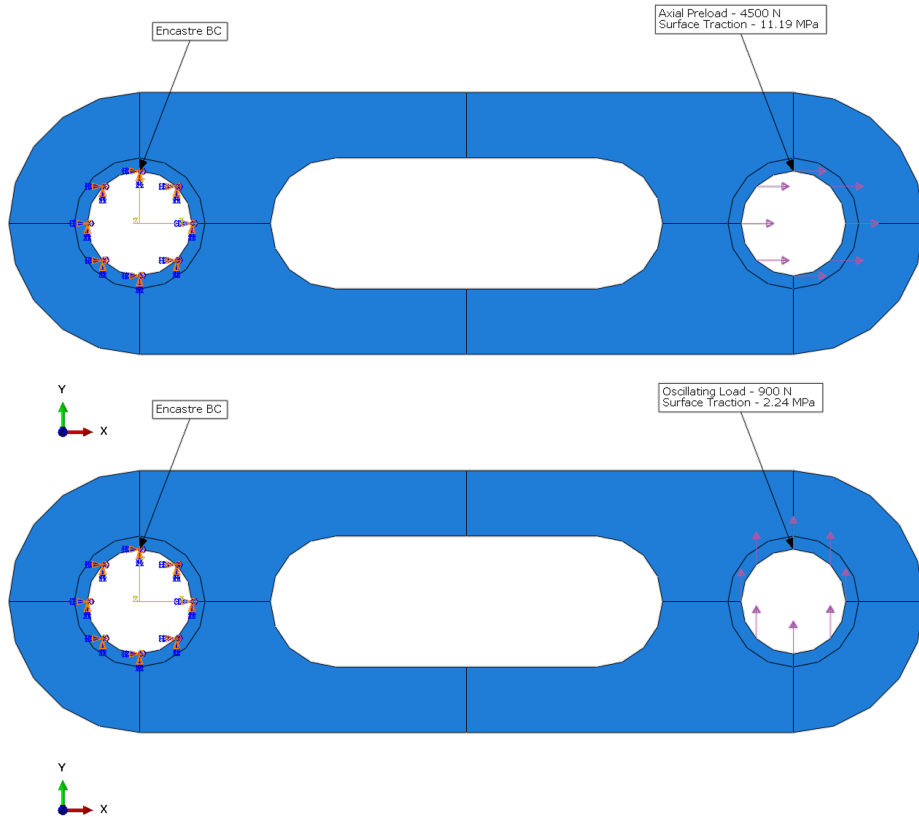


Figure 2: Preload BC and loads shown on top, oscillating BC and loads shown on bottom.

The resulting stresses from the two loading cases are analytically combined in post-processing. The torque arm is modeled as a linear elastic representation of aluminum with Young's Modulus $E = 74.1$ GPa and Poisson's Ratio $\nu = 0.33$. The model is composed of CPS8R elements, 8-node quadratic quadrilateral elements with reduced integration; use of quadratic elements alleviates potential artificial stiffness and more efficiently captures model stresses with a relatively smaller element count than lower-order elements. The *Abaqus CAE* software mesher automatically generates a mesh on the part instances based on a user-defined model element seed size. This approach allows for rapid recreation of meshes for convergence studies.

2 Mesh Convergence

The accuracy of modeling physical phenomena defined by partial differential equations depends heavily on the mesh used to discretize the problem of interest. A mesh convergence study is crucial to maximize the confidence and efficiency of a model. Beginning with a coarse mesh, we analyze the evolution of a specific objective function as the output changes with mesh density across increasingly resolved meshes. *Abaqus* generated a fully-quadrilateral mesh on the torque arm using the medial axis setting to create a uniform, symmetrical mesh. The objective function tracked during the convergence study is maximum Von Mises stress for both the preload and oscillating load conditions. The metric used to increase mesh resolution is element seed size, representative of the approximate final element size in the mesh. Beginning with a seed size of 5 mm, six meshes were created before convergence was achieved for both load cases, using seed sizes of 5, 4, 3, 2, 1, and 0.5. The results of the convergence study are shown in tables 1 and figure 2, both of which highlight the decreasing residual change with increased element count. Increasing resolution beyond the 5th mesh shows a minimal change (< 1%) in maximum Von Mises stress, indicating that the 5th mesh is sufficiently resolved for our analysis and further refinements would only increase computational cost. The initial, converged, and finest meshes are shown in figure 3. Contour plots of Von Mises stress for the initial coarse mesh and final converged mesh, shown in figure 4, show very similar trends with the bulk qualities of the contours in agreement, though the finer details are naturally smoother and more resolved in the converged mesh.

Preload Convergence History						
Mesh Iteration	Seed Size	Number of Elements	Element Type	Element Size (Critical Region)	Von Mises Stress (MPa)	% Change from Previous Mesh
1	5	204	CPS8R	5	57.3	-
2	4	240	CPS8R	4	56.89	-0.72%
3	3	336	CPS8R	3	55.62	-2.23%
4	2	884	CPS8R	2	57.22	2.88%
5	1	3537	CPS8R	1	58.12	1.57%
6	0.5	13801	CPS8R	0.5	58.11	-0.02%

Table 1: Preload mesh convergence history

Oscillating Convergence History						
Mesh Iteration	Seed Size	Number of Elements	Element Type	Element Size (Critical Region)	Von Mises Stress (MPa)	% Change from Previous Mesh
1	5	204	CPS8R	5	138.89	-
2	4	240	CPS8R	4	138.96	0.05%
3	3	336	CPS8R	3	138.81	-0.11%
4	2	884	CPS8R	2	139.84	0.74%
5	1	3537	CPS8R	1	141.85	1.44%
6	0.5	13801	CPS8R	0.5	142.1	0.18%

Table 2: Oscillating mesh convergence history

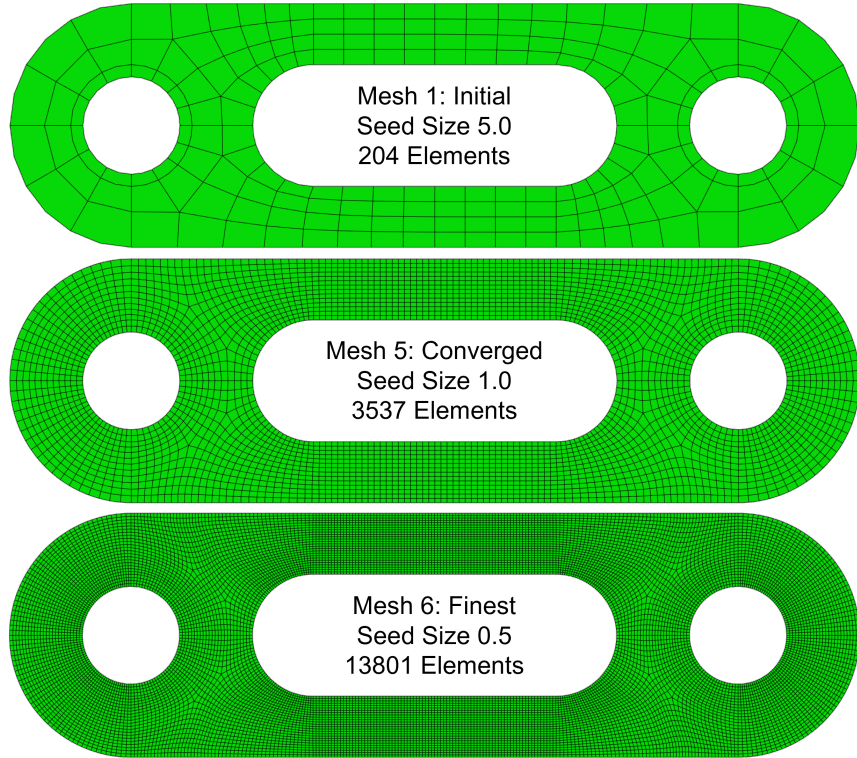


Figure 3: Coarse, converged, and finest mesh.

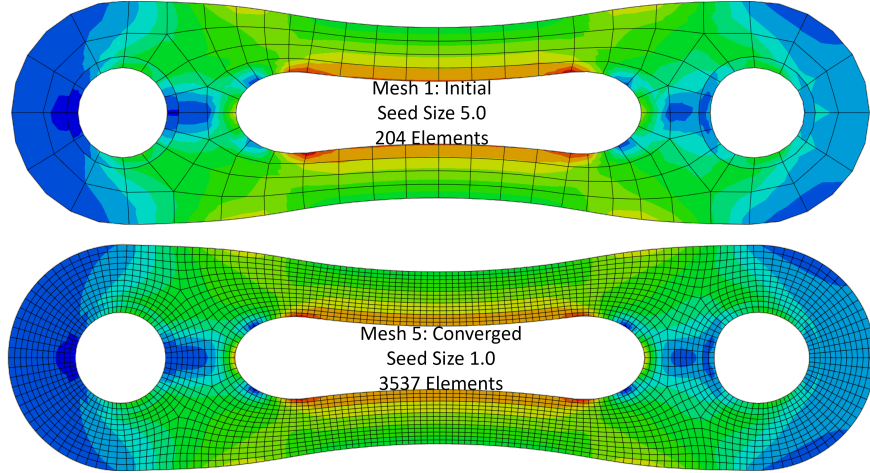


Figure 4: Contour plots of Von Mises stress for initial and converged meshes

3 Results

The torque arm analysis in *Abaqus* uses two distinct loading steps to solve for the stresses generated by the preload and oscillating load conditions. To properly evaluate the performance

of the torque arm under the prescribed loading conditions we combine the stresses of interest after the fact using the built-in post-processing capabilities of the solver. We can verify the chosen modeling assumptions using the same post-processed data. Recall, we have assumed that the critical stresses are not located in the bushings, allowing the part to be modeled with discontinuous thicknesses. The other main modeling assumption is that the details of how the loads are applied are not crucial to understanding the critical stress regions. To verify these assumptions, we examine the contour plots of Von Mises stresses for both cases shown in figures 5-6, noting that the maximum stresses are *not* in the bushing regions, proving that the discontinuous thickness is acceptable. Next, the net reaction force experienced by the torque arm must match the net force of the applied tractions for preload and oscillating steps. The “time” history of reaction forces during analysis steps is plotted in figures 7-8, showing agreement with the applied force magnitudes of 4500 N and 900 N respectively. The reaction forces of -4500 N and -900 N place the torque arm into static equilibrium during the given analysis steps, confirming our second assumption.

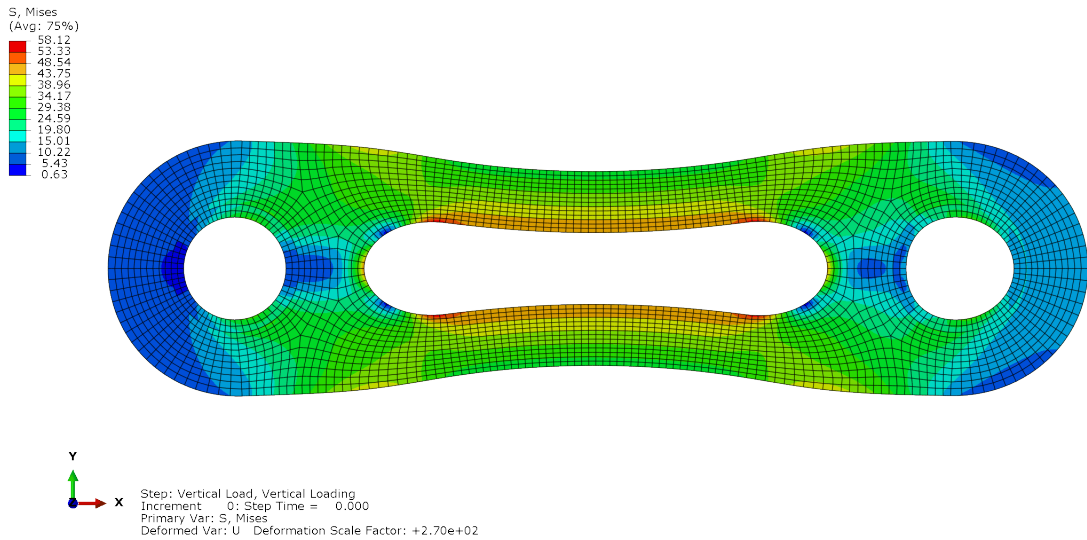


Figure 5: Contours of Von Mises stress for baseline preload

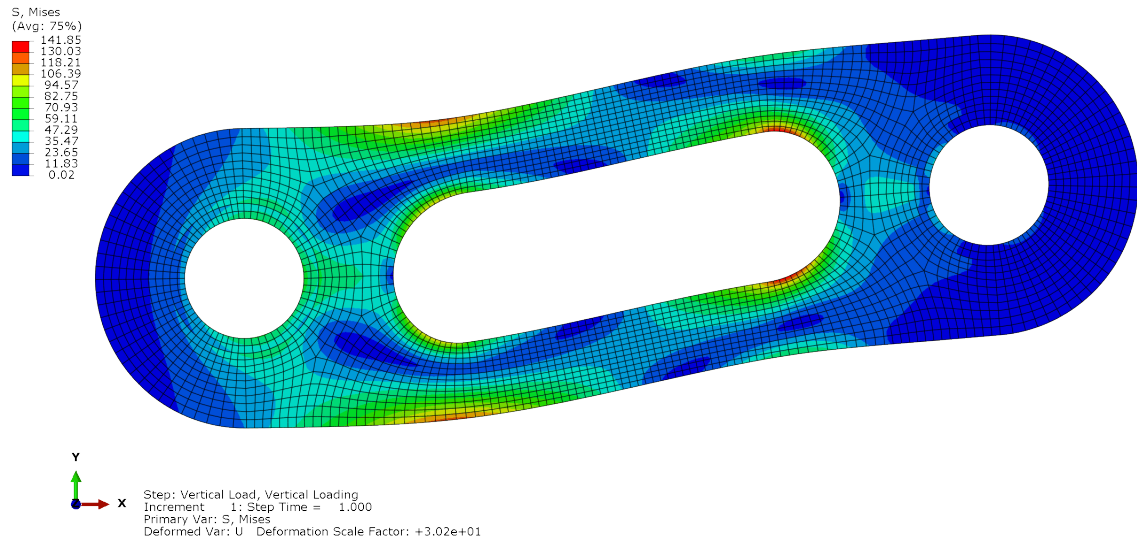


Figure 6: Contours of Von Mises stress for baseline oscillating load

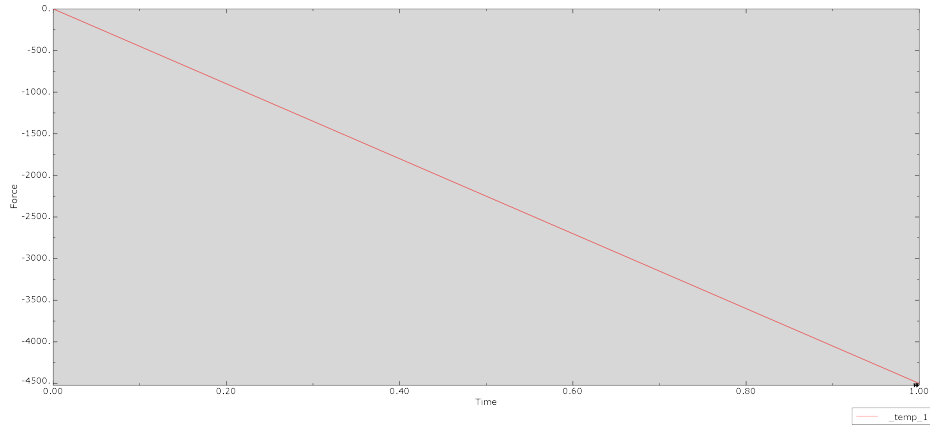


Figure 7: Net reaction force during preload shows agreement with applied load

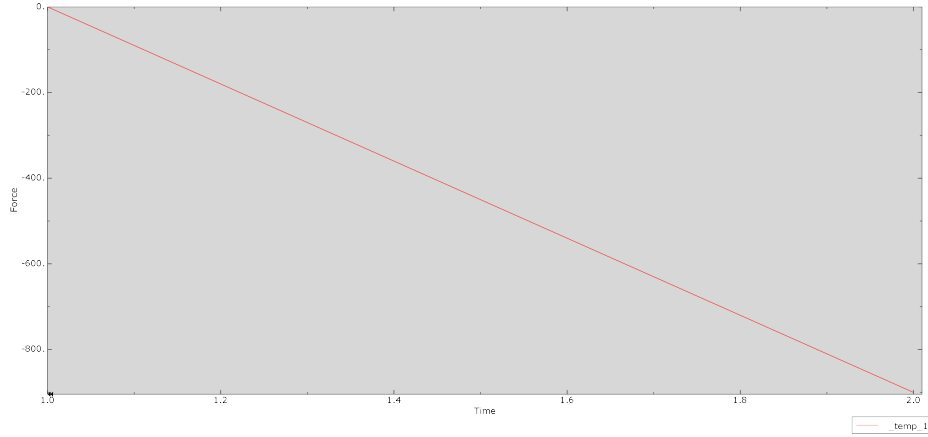


Figure 8: Net reaction force during oscillating load shows agreement with applied load

Having verified the fundamental assumptions made during analysis, we can now evaluate the failure criteria of the torque arm. Given a yield strength of $\sigma_y = 75$ MPa we can check for yield failure by combining the Von Mises stresses from the two loading conditions, shown in figure 9. Adjusting the scale of the contour plots highlights the regions where the stresses exceed the yield strength, shown in figure 10. There are several regions which show signs of yielding and failure with Von Mises stress values substantially larger than the yield strength. The critical region of yielding is located on right side of the torque arm, at the top and bottom of the central gap.

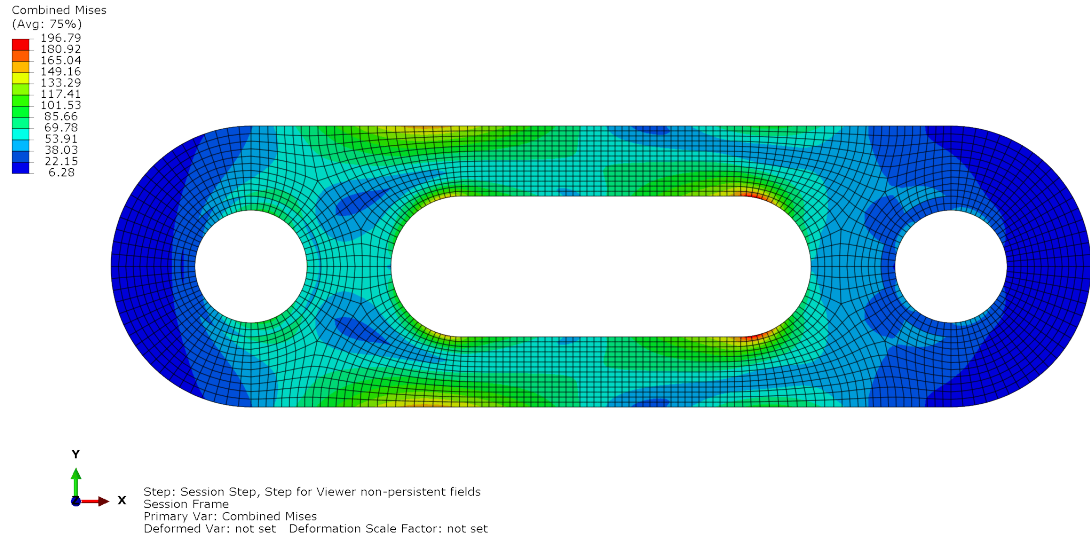


Figure 9: Contour plot of combined Von Mises stresses

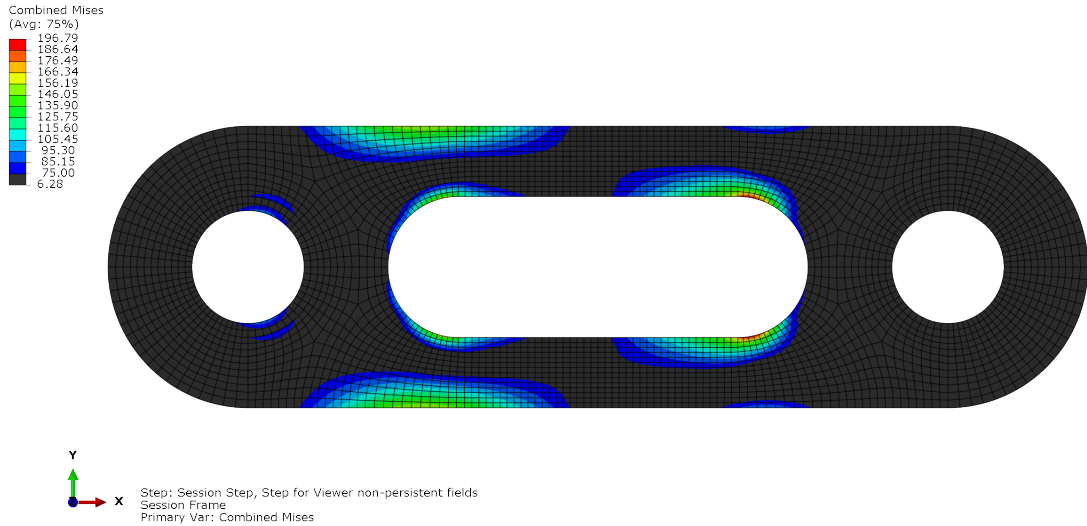


Figure 10: Contour plot of combined Von Mises stresses with failed regions highlighted

To evaluate fatigue failure we utilize the Gerber equation:

$$\frac{\sigma_{cyc}}{\sigma_e} + \left(\frac{\sigma_{mean}}{\sigma_y} \right)^2 = 1$$

By combining the maximum principal stresses from both loading cases we can assess the potential for failure in fatigue. The maximum principal stress from preload and the oscillating load are represented by σ_{mean} and σ_{cyc} , respectively. Similar to the yield strength plots, we can generate a contour plot of the value from the Gerber equation to evaluate the entire torque arm and identify all regions that are likely to fail in fatigue at once, shown in figure 11. Once again in figure 12, by limiting the contour scale we can identify all regions that exceed the Gerber limit of 1. With a peak value of 5.25, the baseline design of the torque arm performs very poorly and requires a dramatic increase in thickness to avoid failure. The critical region for fatigue failure is on the right side of the central gap at the bottom.

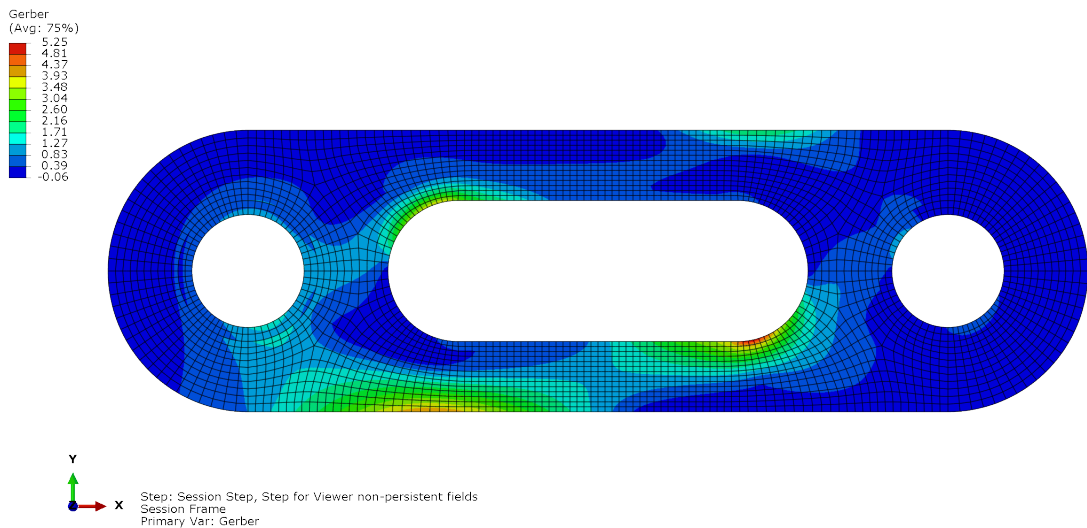


Figure 11: Contour plot of Gerber equation values

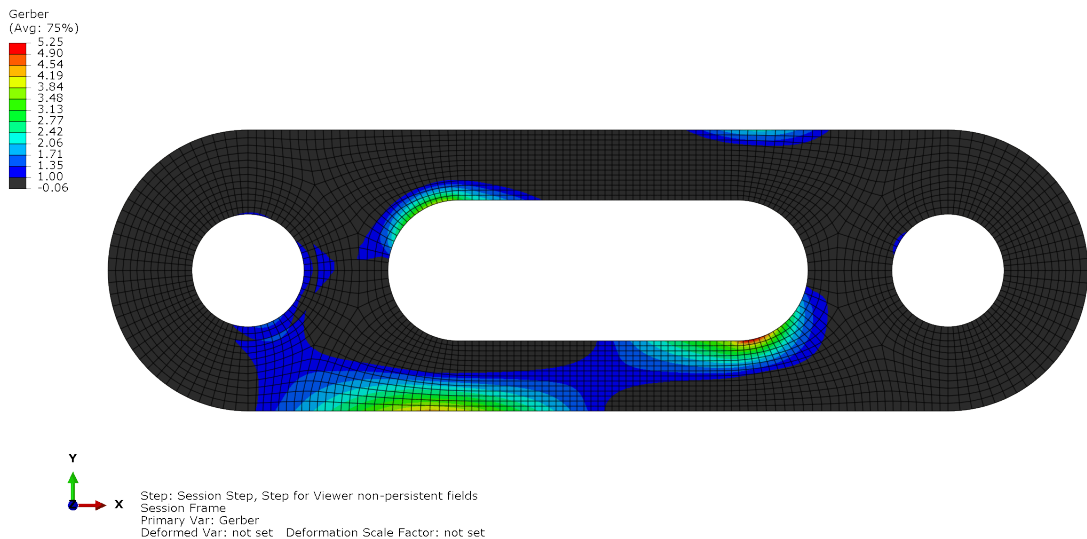


Figure 12: Contour plot of Gerber equation values with failed regions highlighted

4 Redesign

Having proven that the baseline design fails both in yield and in fatigue by significant margins, a redesigned torque arm with increased thickness is required. Note that the peak Gerber value was greater than 5 for the baseline design. A proposed redesign is as follows: increase the thickness of the body and bushing of the torque arm by a factor of 5 each, resulting in a body thickness of 30 mm and a bushing thickness of 40 mm. For this case we maintain the same boundary condition and unique steps for each load case, but adjust the magnitude of the traction so that the constant value of load for each case is maintained. Based on the increased thickness of the bushing, the new tractions for preload and oscillating load are 2.24 MPa and 0.45 MPa respectively. Again, the converged mesh from the baseline is used, with differing thickness represented in the plane stress section property options. The CPS8R element type is also maintained for its speed and accuracy of modeling complex stresses throughout the torque arm.

New Von Mises stress contours for the redesigned part are shown in figures 13-14. The peak magnitude of stress for each step is significantly reduced compared to the baseline design. Note that the contour plots of stresses look identical to the baseline plots, although the maximum values are much smaller. This result is valid for the way we are modeling the problem where the stress values are a direct function of the thickness of the part. The critical stress regions are, once again, not located in the bushing, so our modeling assumptions from the baseline case hold equally valid.

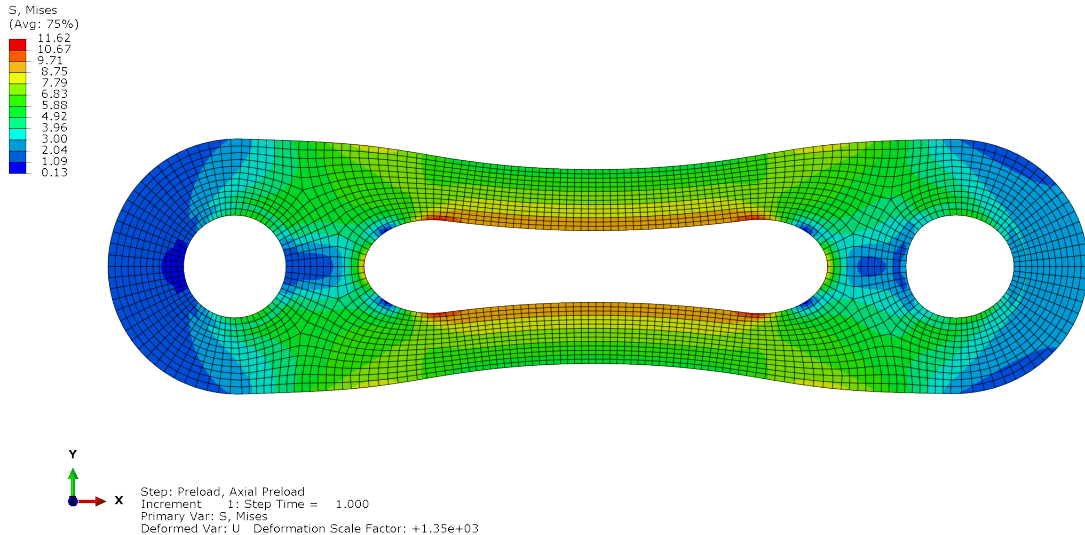


Figure 13: Contours of Von Mises stress for redesigned preload

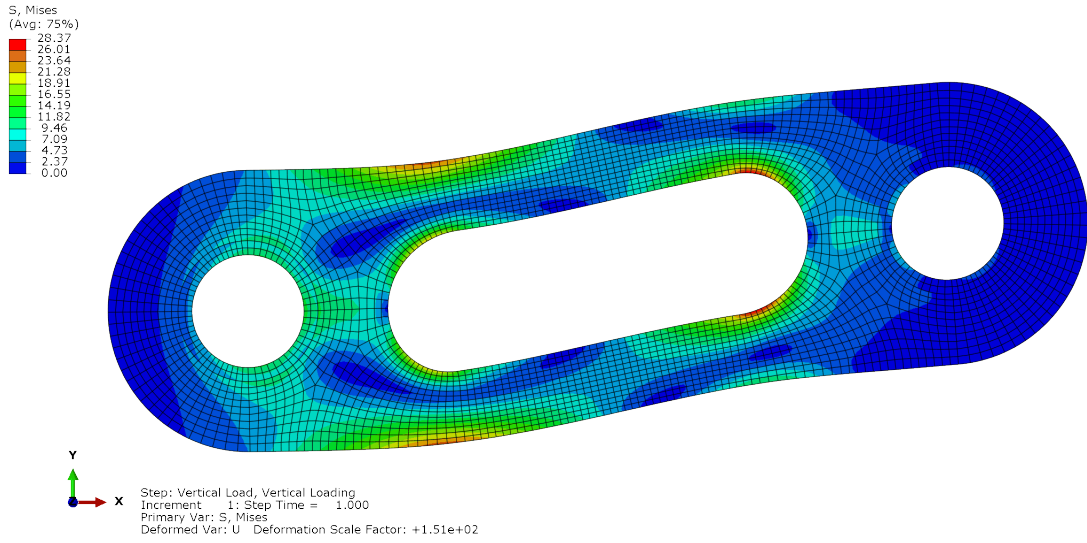


Figure 14: Contours of Von Mises stress for redesigned oscillating load

Next, we examine the torque arm's yield performance. Combining the Von Mises stress contours again and comparing to the yield strength, we see that the redesigned part does not experience a failure from yield, with all stresses below 75 MPa. The maximum stresses occur in the same locations as the baseline design with a reduced amplitude, shown in figure 15.

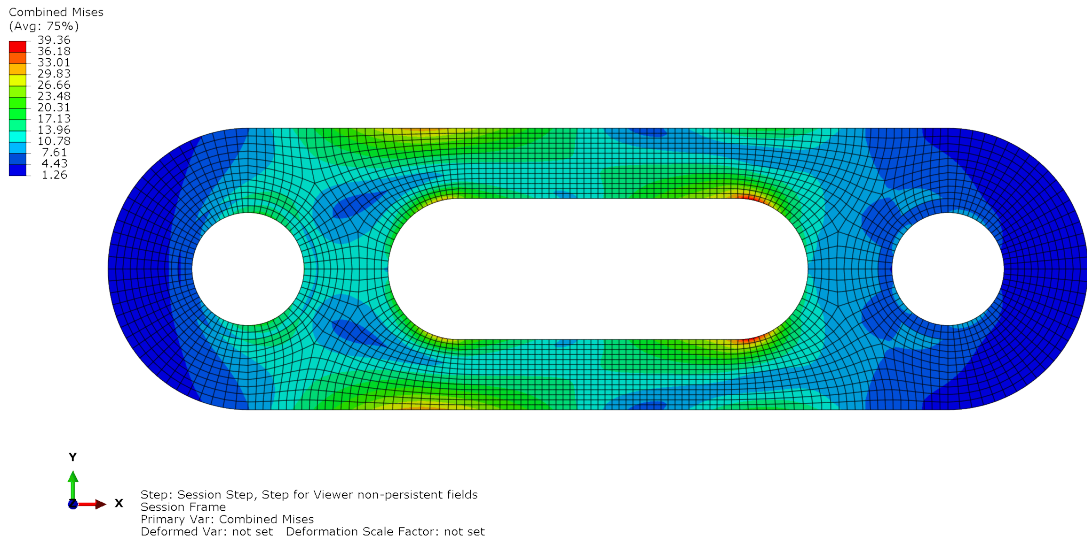


Figure 15: Contour plot of combined Von Mises stresses on redesigned model

The baseline design was much more likely to fail from fatigue than from yield, so evaluation of the Gerber values for the redesigned part is especially important. Figure 16 shows a peak Gerber value of 0.97, 3% from the limit of 1. The redesigned part is overly strong in yield but fairly close to the fatigue design limit. A fatigue failure would appear at the bottom right of the center gap, where the peak value of 0.97 is observed.

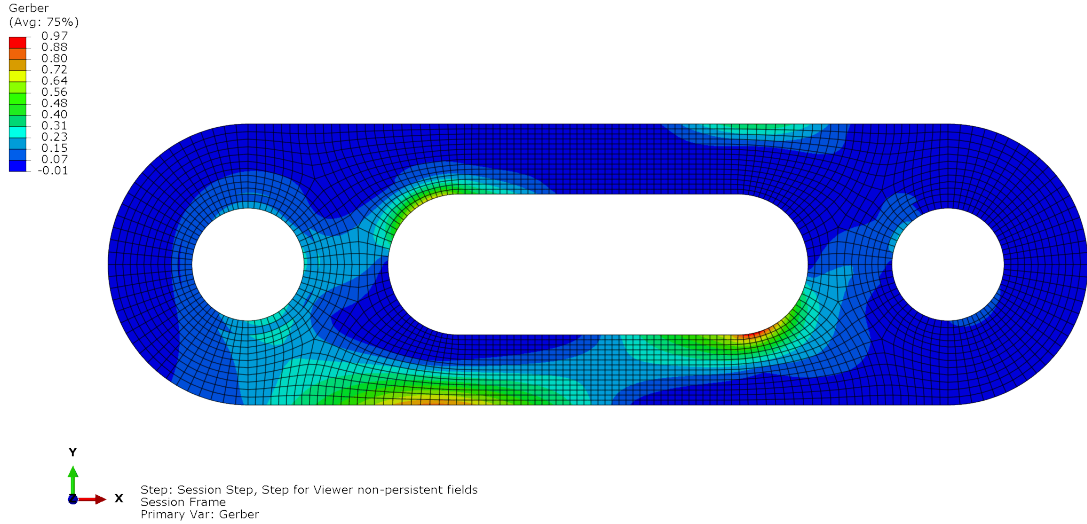


Figure 16: Contour plot of Gerber equation values on redesigned model

Based on the Von Mises and Gerber criteria examined we have redesigned the part to no longer experience the same failure modes of the baseline. The redesigned part has a safety factor of $n = 1.02984$, indicating that it is very close to the failure threshold (for details, see appendix B). The thickness increases a dramatic amount and a better method of redesign could potentially be to use a different material with a larger modulus of elasticity. However, if the part is primarily weight-constrained rather than volume constrained, an increase in thickness may be a valid avenue rather than using a denser material.

5 Summary and Conclusions

We modeled a torque arm in the finite element software *Abaqus* using a 2D plane stress approach to evaluate the potential for failure in yield and fatigue from a constant axial preload and an oscillating vertical load. The baseline model was shown to fail both in yield and in fatigue with critical regions located at the right side of the center gap in the torque arm. Failure in yield was evaluated using the combined Von Mises stresses from the axial preload while failure in fatigue was evaluated using the Gerber equation to look at the impact of

a mean load and oscillating load on the part. By increasing the thicknesses of the torque arm by a factor of 5, the part no longer fails by yield or fatigue. The redesigned torque arm experiences reduced peak stresses compared to the baseline model and is over-designed for yield failure but has a peak Gerber value of 0.97, 3% below the fatigue failure criteria.

We made several critical assumptions in the process of modeling the torque arm and its loads, namely the choice to use a plane stress model, the discontinuous thicknesses in the part geometry, and the method of applying loads via general tractions. The part could have been modeled in 3D space at a higher computational cost with more complex element requirements, but for our purposes using the 8-node quadratic quadrilateral elements was sufficient to capture the peak stresses of interest. By carrying out a mesh resolution study, we feel confident having captured the critical stresses of interest both for the baseline and redesigned parts. The encastre boundary condition on the left hole of the torque arm is potentially overly constrained but because the critical stresses are not experienced near that boundary region, we can again neglect the finer details of stresses near the boundary condition.

Appendix A References

Cook, Robert D., Malkus, David S., Plesha, Michael E. and Witt, Robert J.. Concepts and Applications of Finite Element Analysis, 4th Edition. 4 : Wiley, 2001.

Whitney, Thomas. Finite Element Analysis I - AEE 546 Lectures, Fall 2022.

ABAQUS Online Documentation: Version 6.6-1

Appendix B Safety Factor Calculation

The Gerber equation with safety factors included:

$$\frac{n_s \sigma_{cyc}}{\sigma_e} + \left(\frac{n_s \sigma_{mean}}{\sigma_y} \right)^2 = 1$$

From the redesigned part:

$$\sigma_{cyc} = 28.29 \text{ MPa}$$

$$\sigma_e = 30 \text{ MPa}$$

$$\sigma_{mean} = 11.62 \text{ MPa}$$

$$\sigma_y = 75 \text{ MPa}$$

Substituting in and generating a quadratic in terms of n_s :

$$0.9463n_s + 0.024n_s^2 = 1$$

Solving for the positive value of n_s :

$$n_s = 1.02984$$